Springer

KSME

Journal of Mechanical Science and Technology 24 (11) (2010) 2181~2188
www.springerlink.com/content/1738-494x
DOI 10.1007/s12206-010-0812-7

Dynamic analysis of a train-bridge system under multi-support seismic excitations †

Nan Zhang[1,2,*], He Xia[1] and Guido De Roeck[2]

[1]*School of Civil Engineering, Beijing Jiaotong University, Beijing 100044, China*
[2]*Department of Civil Engineering, Catholic University of Leuven, Heverlee B-3001, Belgium*

(Manuscript Received March 23, 2010; Revised June 18, 2010; Accepted July 12, 2010)

Abstract

A numerical solution for the dynamic responses of a train-bridge interaction system subjected to multi-support seismic loads was studied. The train vehicle was modeled by the rigid-body dynamics method, and the bridge was modeled by the finite element method. The vertical and lateral wheel-rail interaction forces were defined according to the wheel-rail corresponding assumption and the simplified Kalker creep theory. Three-dimensional seismic accelerations were incorporated using the large mass method. In a case study, the dynamic responses were simulated for a high-speed train traversing a steel truss cable-stayed bridge with different seismic intensities and different train speeds, and train safety was evaluated.

Keywords: Cable-stayed bridge; Multi-support excitations; Seismic load; Vehicle-bridge interaction system

1. Introduction

Railway bridge span lengths have increased significantly in recent years, and additional kilometers of elevated bridges have been added to modern high-speed railway systems [1-3]. This, not to mention the several recent reports of bridge-traversing train derailments during earthquakes [1], calls for more research attention to be paid to the safety of vehicle-bridge systems under seismic excitations.

In most studies on this subject, the dynamic responses of vehicle-bridge systems under seismic loads have been analyzed using the numerical history integral method, the given ground-motion histories having been inputted into the interaction system. Here, the seismic load is defined as the product of the global mass matrix and the seismic acceleration vector, according to the consistent seismic excitation method (CSEM). In the CSEM, identical acceleration histories have to be incorporated for all of the bridge nodes, which practice is far from satisfactory given that under real boundary conditions, the phase angles of seismic waves differ for different foundations, especially in the case of long-span bridges.

As a remedy for the shortcomings of the CSEM, the adoption of multi-support seismic excitation allows for inputting of different seismic displacements, velocities or accelerations for different bridge foundations. There are several ways to allow bridge foundations to have various motion histories in the time domain, such as the relative motion method (RMM) [4-6], the large mass method (LMM) [7] and the large spring method (LSM) [8]. The RMM, based on the superposition of the quasi-static response and the dynamic response, is not suitable for finite element method (FEM) calculation, whereas the seismic acceleration is incorporated by the LMM, and the seismic displacement, by the LSM.

There are also frequency domain methods, such as the multi-support response spectrum method (MSRS) [9-12] and the pseudo-excitation method (PEM), that have been adopted for both research and engineering cases [13]. However, neither the MSRS nor the PEM is adequate for a vehicle-bridge interaction study, owing to the fact that it is difficult to obtain the wheel-rail interaction force in the frequency domain.

The vehicle-bridge interaction system has been studied for several decades. In contrast to systems omitting earthquake excitation, the vehicle-bridge interaction system with seismic load has the following characteristics:

(1) The relative motion between the wheel and rail will be much larger, so the wheel-rail interaction assumption must be operative in cases of large deformation;
(2) The seismic force between the wheel and rail can be quite large, so the time step of the numerical integral must be much smaller to ensure time iteration convergence;
(3) The riding comfort requirement on train vehicles can be ignored when earthquake occurs.

The present study was undertaken with the aim of establishing a method to predict the dynamic responses of the vehicle-bridge interaction system, in which bridge foundations can

† This paper was recommended for publication in revised form by Associate Editor Won-Gu Joo

*Corresponding author. Tel.: +86-10-51683786, Fax: +86-10-51683340
E-mail address: nzhang@bjtu.edu.cn

incorporate various seismic motion histories. The main goal of this study was to prevent bridge-traversing trains from derailing when earthquakes occur; the possibilities or effects of bridge damage were not considered.

2. Vehicle-bridge interaction model

The vehicle-bridge interaction model consists of the vehicle subsystem and the bridge subsystem, which are linked by the assumed wheel-rail interaction. The seismic ground acceleration and the track irregularity are taken as system excitations.

The coordinate systems for both of the two subsystems are defined as follows: X denotes the train-running direction, Z the downward and Y the lateral (as determined by the Right-hand rule); RX, RY and RZ denote the rotational directions with respect to the axes X, Y and Z, respectively.

2.1 Vehicle model

The motion equations of the vehicle subsystem can be expressed as

$$\mathbf{M}_V\ddot{\mathbf{X}}_V + \mathbf{C}_V\dot{\mathbf{X}}_V + \mathbf{K}_V\mathbf{X}_V = \mathbf{P}_V \tag{1}$$

where $\mathbf{M}_V$, $\mathbf{C}_V$, and $\mathbf{K}_V$ are the mass, damping and stiffness matrices, respectively, $\mathbf{X}_V$ is the displacement vector, and $\mathbf{P}_V$ is the force vector of the vehicle subsystem. The force vector $\mathbf{P}_V$ contains the wheel-rail interaction forces acting on the vehicle subsystem (these forces are discussed in Section 2.4).

The following assumptions are adopted in modeling the vehicle subsystem:

(A1) The train is composed of several independent vehicle elements, and thus the global mass, damping and stiffness matrices of the vehicle subsystem can be assembled diagonally by the corresponding matrices of each element, and the global displacement and force vectors of the vehicle subsystem can be assembled by the vectors of each element.

(A2) For high-speed trains, each vehicle element consists of one car-body, two bogies and four wheel-sets. The car-body and the bogies are linked by the second suspension system, and the bogies and the related wheel-sets are linked by the first suspension system. The suspension systems comprise springs and dampers, as shown in Fig. 1.

(A3) Each car-body or bogie has 5 DOFs (degrees-of-freedoms) in the Y, Z, RX, RY and RZ directions.

(A4) Each wheel-set has 3 DOFs in the Y, Z and RX directions. There is no relative displacement, velocity or acceleration between the wheel-sets and the track in the vertical direction, so the Z and RX DOFs of the wheel-set are dependent.

Thus a vehicle element has 19 independent DOFs and 8 dependent DOFs. The mass matrix $\mathbf{M}_A$, damping matrix $\mathbf{C}_A$ and stiffness matrix $\mathbf{K}_A$ of a vehicle element can be derived by the Lagrange Equation or dynamic equilibrium conditions [14].

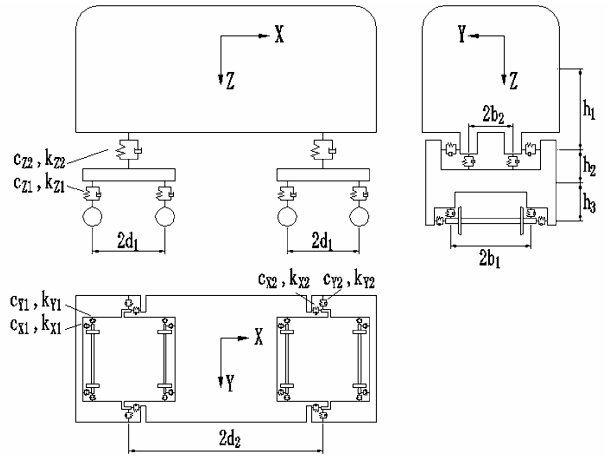

Fig. 1. Vehicle model.

2.2 Bridge model and seismic excitations

Because the seismic load is induced by ground accelerations, the multi-support seismic excitations are incorporated into the bridge foundations by the large mass method (LMM), in which the DOFs of the multi- support excitations are considered free, and the mass, damping and stiffness matrices of the bridge subsystem can be obtained by the FEM. The motion equations of the bridge subsystem can be expressed as

$$\left(\mathbf{M}_B + \mathbf{M}_L\right)\ddot{\mathbf{X}}_B + \mathbf{C}_B\dot{\mathbf{X}}_B + \mathbf{K}_B\mathbf{X}_B = \mathbf{P}_B + \mathbf{M}_L\mathbf{A}_G \tag{2}$$

where $\mathbf{M}_B$, $\mathbf{C}_B$ and $\mathbf{K}_B$ are the mass, damping and stiffness matrices of the bridge subsystem, containing the DOFs of multi-support excitations; $\mathbf{X}_B$ and $\mathbf{P}_B$ are the displacement and the force vectors of the bridge subsystem, and $\mathbf{M}_L$ and $\mathbf{A}_G$ are the large mass matrix and the seismic acceleration vector, defined as

$$\mathbf{M}_L = \begin{bmatrix} 0 & & & & 0 \\ & m_D & & & \\ & & 0 & & \\ & & & m_D & \\ 0 & & & & \ddots \end{bmatrix} \tag{3}$$

$$\mathbf{A}_G = \begin{bmatrix} 0 & a_{G,N1} & 0 & a_{G,N2} & \cdots \end{bmatrix}^{\mathrm{T}} \tag{4}$$

The non-zero elements in $\mathbf{M}_L$ and $\mathbf{A}_G$ are in the row/column corresponding to the DOF of the multi-support excitations, m_D is a large mass linked to the concerned DOFs (N_1, N_2,…) and can be set as 10^3 to 10^5 times the structure mass, and $a_{G,Ni}$ is the seismic acceleration of the N_ith DOF in the bridge subsystem.

The force vector $\mathbf{P}_B$ in Eq. (2) contains the wheel-rail interaction force and the static wheel loads, and is discussed in Section 2.4.

It is interesting to note that the bridge subsystem might become an indeterminate structure when the excited supports are

set free; however, Eq. (2) can still be solved, due to the large mass matrix $\mathbf{M}_L$. Of course, an excessively large value of m_D might induce a large error in calculation, and therefore must be avoided.

2.3 Rail irregularity excitations

The rail irregularity reflects the relative displacement between the wheel and rail. It can cause additional velocity and acceleration, which can be expressed in a differential form. For example, the additional velocity and additional acceleration of vertical irregularity Z_I can be expressed as

$$\dot{Z}_I = \lim_{\Delta t\to 0}\frac{\Delta Z_I}{\Delta t} = V\cdot\lim_{\Delta t\to 0}\frac{\Delta Z_I}{\Delta X} = V\cdot\frac{\partial Z_I}{\partial X} \tag{5}$$

$$\ddot{Z}_I = \lim_{\Delta t\to 0}\frac{\Delta \dot{Z}_I}{\Delta t} = V\cdot\lim_{\Delta t\to 0}\frac{\Delta \dot{Z}_I}{\Delta X} = V^2\cdot\frac{\partial^2 Z_I}{\partial X^2} \tag{6}$$

where V is the train speed.

2.4 Wheel-rail interaction

The vertical wheel-rail interaction force is defined by the assumption (A4) in Section 2.1 called the wheel-rail corresponding assumption. The lateral wheel-rail force is defined by the following:

(A5) The wheel-rail interaction obeys the Kalker creep theory, namely, the interaction force is in proportion to the relative velocity between the wheel and rail.

The vertical and lateral wheel-rail interaction forces for an individual wheel-set are shown in Fig. 2. In the figure, the displacements of suspension points 1, 2, 3 and 4 are defined as

$$\begin{cases} Z_{1,2} = Z_J - id_1R_{YJ} \mp b_1R_{XJ} \\ Z_{3,4} = Z_D + Z_I \mp b_1R_{XI} \\ Z_I = \dfrac{Z_{IL}+Z_{IR}}{2} \\ R_{XI} = R_{XD} + \dfrac{Z_{IR}-Z_{IL}}{g_0} \end{cases} \tag{7}$$

where g_0 is the track gauge, d_1 and b_1 are illustrated in Fig. 1, i=1 for the front wheel-set and i=-1 for the rear wheel-set, Z_J, R_{XJ} and R_{YJ} are the bogie displacements in the Z, RX and RY directions, Z_D and R_{XD} are the deck displacement in the Z and RX directions, and Z_{IL} and Z_{IR} are the vertical irregularities of the left and right rail, respectively. Thus the forces F_1 and F_2 in the first suspension system are

$$\begin{cases} F_1 = k_{Z1}(Z_1 - Z_3) + c_{Z1}(\dot{Z}_1 - \dot{Z}_3) \\ F_2 = k_{Z1}(Z_2 - Z_4) + c_{Z1}(\dot{Z}_2 - \dot{Z}_4) \end{cases} \tag{8}$$

where k_{Z1} and c_{Z1} are the spring and damping coefficients of the first suspension system, as shown in Fig. 1. The vertical

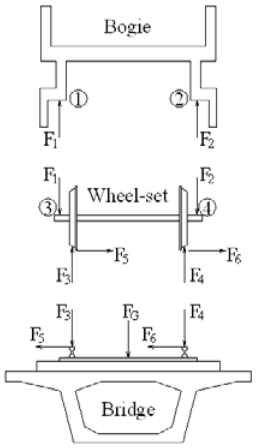

Fig. 2. Wheel-rail interaction.

wheel-rail interaction forces F_3 and F_4 can be calculated according to the equilibrium conditions as

$$F_{3,4} = \frac{m_0\ddot{Z}_I + F_1 + F_2}{2} \mp \frac{I_{X0}\ddot{R}_{XI} + b_1(F_1 - F_2)}{g_0} \tag{9}$$

where m_0 and I_{X0} are the mass and the X inertia of the wheel-set.

The motion equations of the vehicle subsystem are established with respect to the equilibrium position in the vertical direction, so the gravity forces themselves need not be taken into account. But for the bridge subsystem, the gravity load of the vehicle, expressed by F_G, and acting at the mid-point of the two rails, must be considered, as shown in Fig. 2.

The lateral forces F_5 and F_6 in Fig. 2 can be expressed by the Kalker creep theory in the form

$$F_{5,6} = -\frac{f_{22}(\dot{Y}_W - \dot{Y}_D - \dot{Y}_{IL,IR})}{V} \tag{10}$$

where Y_W is the Y displacement of the wheel-set, Y_D is the Y displacement at the mid-point of the rails on the bridge deck; Y_{IL} and Y_{IR} are the lateral irregularities of the left and right rail, respectively, and f_{22} is the creep coefficient, which is a function of (1) the radius of the wheel-set; (2) the curvature radius of the wheel-set at the wheel-rail contact point; (3) the curvature radius of the rail at the wheel-rail contact point, and (4) the wheel-rail normal force.

It can be determined by the analytic geometry method that the curvature radius of the contact point for the wheel and rail are infinity and 300 mm, respectively [15]. Based on the results obtained in [16], the wheel-rail normal contact force, differing very little in time history, and can be regarded as a static wheel weight. Then, the creep coefficient f_{22} is a constant for a given wheel-set.

Thus the wheel-rail interaction force vector $\mathbf{P}_V$ in Eq. (1), or $\mathbf{P}_B$ in Eq. (2), can be obtained by summing the interaction forces F_3 to F_6 of each individual wheel-set.

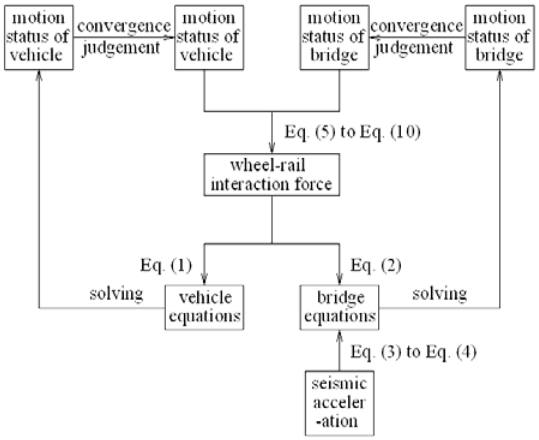

Fig. 3. Iteration process within each time step.

2.5 Equations of motion

The simultaneous equations of the vehicle-bridge interaction system can be established by Eq. (1) and Eq. (2) as

$$\begin{cases} \mathbf{M}_V\ddot{\mathbf{X}}_V + \mathbf{C}_V\dot{\mathbf{X}}_V + \mathbf{K}_V\mathbf{X}_V = \mathbf{P}_V \\ (\mathbf{M}_B + \mathbf{M}_L)\ddot{\mathbf{X}}_B + \mathbf{C}_B\dot{\mathbf{X}}_B + \mathbf{K}_B\mathbf{X}_B = \mathbf{P}_B + \mathbf{M}_L\mathbf{A}_G \end{cases} \quad (11)$$

The equations of motion can be solved by a numerical history integral method such as the Newmark-β method. There are two subsystems in Eq. (11), where $\mathbf{P}_V$ and $\mathbf{P}_B$ are both functions of $\mathbf{X}_V$, $\mathbf{X}_B$ and their differential forms; to ensure that the solution satisfies the equations, an iteration process is performed within the time step, as shown in Fig. 3.

The simultaneous equations (Eq. (11)) are composed of two coupled subsystems. Although they are strictly a conditional convergent process, the unconditional integral method nonetheless can be approximately used, based on the conclusions drawn in [17]. Therefore, in some cases, the choice of the time step is critical.

3. Case study

The dynamic responses of the CRH2 train traversing the Anqing Yangtse River Bridge were simulated in a case study. The samples in the space domain transformed by the German Low Disturbing Track Spectra were chosen as the track irregularities. The three-dimensional seismic acceleration histories, the Tianjin Waves recorded on November 25, 1976, were taken as seismic excitations.

3.1 Outline of Anqing Yangtse River Bridge

The Anqing Yangtse River Bridge is a double-track, steel truss cable-stayed bridge with spans of 101.5+188.5+580+ 217.5+ 159.5+116 m. The bridge towers are 210 m in height, on which the stiffening beam is stayed with 144 cables. The cross-section of the stiffening beam is 15 m in height and 24 m in width. The elevation and cross-section of the bridge are shown in Figs. 4 and 5, respectively.

Table 1. Natural frequencies and modes of bridge.

No.	Freq. /Hz	Modes
1	0.153	Beam, lateral symmetrical
2	0.334	Beam, vertical symmetrical
3	0.353	Beam, lateral asymmetrical
4	0.388	Beam, vertical asymmetrical
5	0.389	Tower, lateral

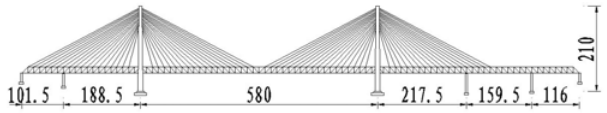

Fig. 4. Elevation of bridge (m).

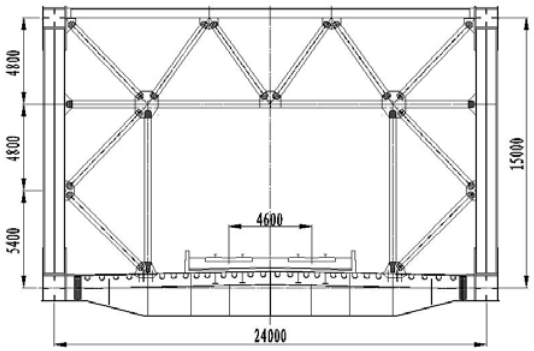

Fig. 5. Cross-section of stiffening beam (mm).

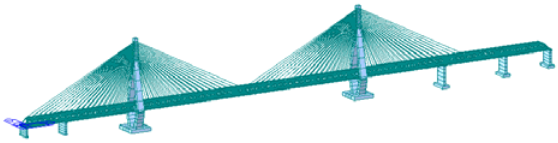

Fig. 6. FEM model of bridge.

The bridge model displayed in Fig. 6 was derived by the FEM, according to which the bridge members, towers and piers were modeled with spatial beam elements, the cables with truss elements, and the seven foundations of the bridge were treated as free nodes. The total mass of the bridge is about 4×10^8 kg; m_D in Eq. (3) was set as 10^{12} kg.

The first 5 natural frequencies and modes of the bridge are listed in Table 1.

3.2 Information on CRH2 train

The CRH2 high-speed train consists of 8 vehicles, MTMTTMTM, where M stands for the motored-tractors and T, the trailers. The static loads of the tractors and trailers are 135 kN and 120 kN, respectively. Both the tractors and trailers are 25 m in length. The natural frequencies of the tractor are

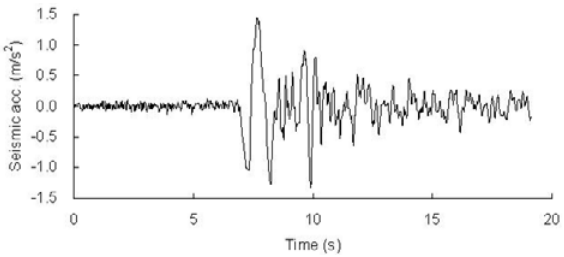

(a) north-south

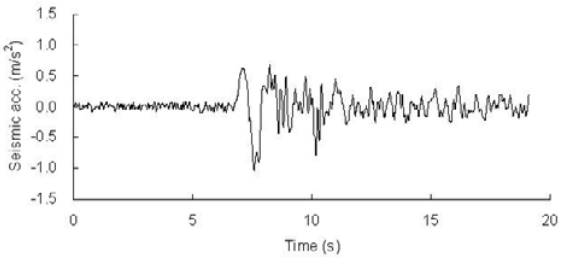

(b) east-west

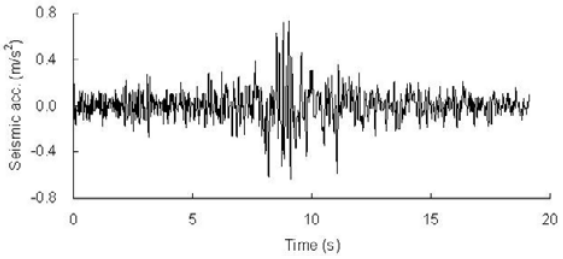

(c) vertical direction

Fig. 7. Acceleration histories of Tianjin seismic waves.

1.621 Hz in vertical vibration and 1.676 Hz in lateral, and those of the tailor are 1.788 Hz and 1.860 Hz, respectively.

3.3 Parameters of track irregularity

The samples in the space domain transformed by the German Low Disturbing Track Spectra were chosen as the track irregularities, with wavelengths ranging from 1m to 80m, subject to the maintenance conditions of the bridge.

3.4 Parameters of seismic accelerations

Measured seismic accelerations, the three-dimensional histories in Tianjin Waves, recorded on November 25, 1976, were chosen as the seismic excitations. The parameters of the Tianjin Waves are listed in Table 2, and the original seismic acceleration records are shown in Fig. 7.

In order to simulate the responses of the different seismic intensities, the Tianjin Waves were normalized with the peak values of the seismic intensities V, VI and VII [1], where the vertical peaks are set as half of the two horizontal ones (see Table 3). The records for the north-south, east-west and vertical directions were incorporated as the X, Y and Z axes, respectively.

Table 2. Parameters of Tianjin Waves.

Items	Value
Seismic intensity	6.9
Distance to epicenter	65 km
Effective frequency band	0.3-35 Hz
Peak acceleration, north-south	1.458 m/s2
Peak acceleration, east-west	1.042 m/s2
Peak acceleration, vertical direction	0.731 m/s2

Table 3. Peak seismic acceleration values.

Item	Peak acceleration (m/s^2)		
	X	Y	Z
SI V	0.310	0.310	0.155
SI VI	0.630	0.630	0.315
SI VII	1.250	1.250	0.625

SI=Seismic Intensity

The three-dimensional seismic wave speed was taken as 3000 m/s. It was assumed that the seismic waves propagated in the X direction; thus the time difference between the first foundation and the other 6 were 0.034s, 0.097 s, 0.290 s, 0.363 s, 0.416 s and 0.454 s, respectively.

3.5 Bridge responses

Mid-span displacements and accelerations in the lateral and vertical directions were studied. All of the cases were calculated for a train speed ranging from 150 km/h to 350 km/h and the seismic intensities V, VI and VII. To study the effect of earthquakes, the responses without seismic loads also were calculated.

The typical displacement and acceleration histories of the bridge at mid-span are shown in Figs. 8 and 9, respectively, where the thicker lines stand for the response without seismic load and the thinner lines stand for the response with seismic intensity V. All of the histories are for train speeds under 300 km/h.

The bridge responses versus train speed for different seismic intensities are shown in Figs. 10 and 11, where "none" stands for the response without seismic load.

It was calculated that the first and last wheel-sets passed the bridge mid-span at times 8.16 s and 11.70 s respectively, between which the acceleration histories contain more high-frequency vibration components, due to the effect of track irregularity. This phenomenon also implies that bridge vibration induced by seismic excitations has a lower-frequency component than that induced by track-irregularity excitations.

The lateral displacement and acceleration evidently increased when the seismic load was incorporated; however, for the vertical displacement and acceleration, there were very small differences between the with- and without-seismic-load histories. The reason was that the vertical response of the

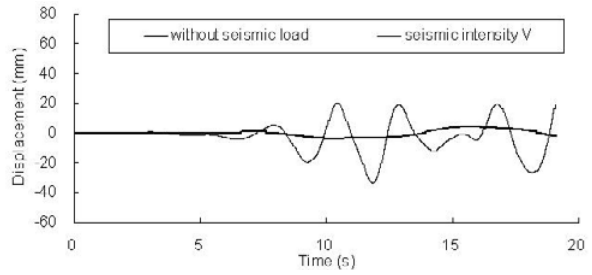

(a) lateral

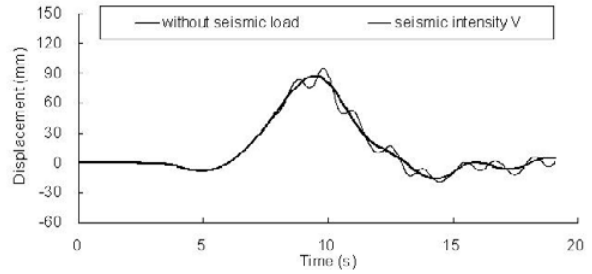

(b) vertical

Fig. 8. Mid-span displacement histories.

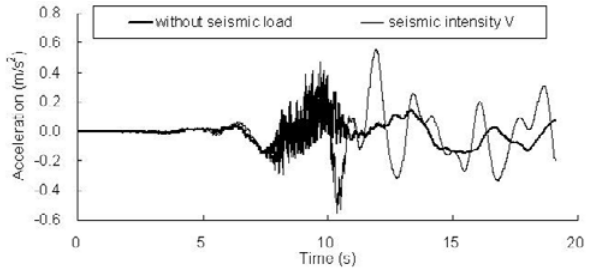

(a) lateral

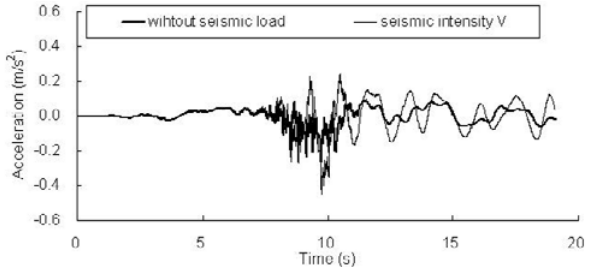

(b) vertical

Fig. 9. Mid-span acceleration histories.

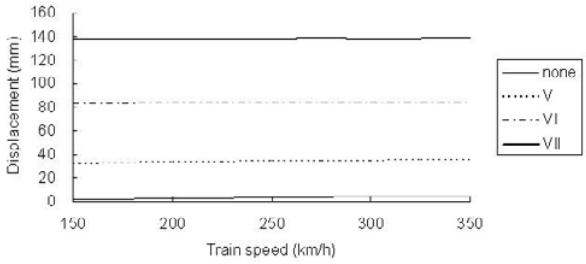

(a) lateral

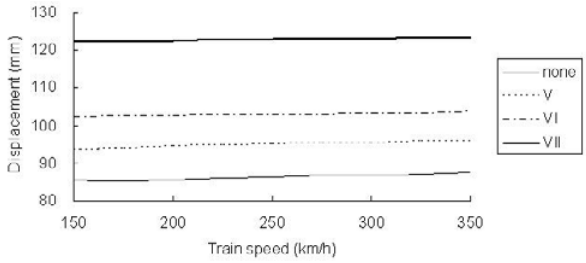

(b) vertical

Fig. 10. Maximum mid-span displacements vs. train speed.

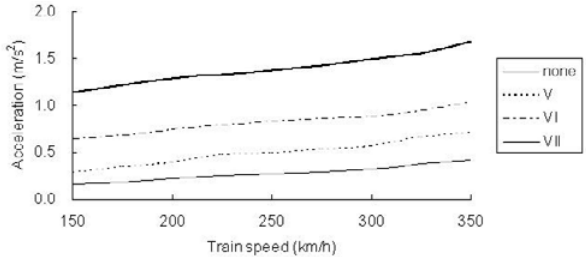

(a) lateral

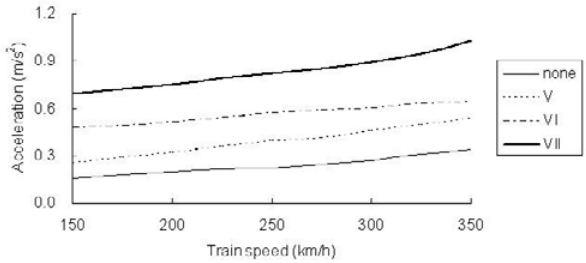

(b) vertical

Fig. 11. Maximum mid-span accelerations vs. train speed.

bridge subsystem is determined mainly by the axis weight of the vehicle, whereas the seismic excitations and track irregularity make relatively only small contributions.

Figs. 10 and 11 also show that all of the mid-span responses increased with train speed, with or without seismic load. Further, the bridge response was very sensitive to the seismic intensity, which also proves that earthquake excitation makes a larger contribution than track-irregularity excitation to the vehicle-bridge interaction system. The lateral response of the bridge was roughly in proportion to the seismic acceleration, whereas the differences among the vertical responses were relative small due to the effect of the train's gravity load.

3.6 Vehicle response

It is known that derailment and overturning of trains are the most common accidents when earthquake occurs. For the purpose of evaluating the safety of vehicles, the typical lateral and vertical wheel-rail interaction forces for speeds under 300 km/h were determined, and the results plotted in Figs. 12 and 13.

The figures show some low-frequency force components ex-

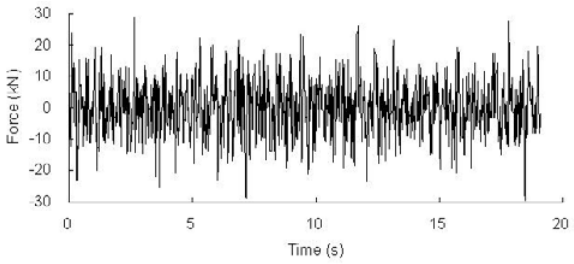

(a) without seismic load

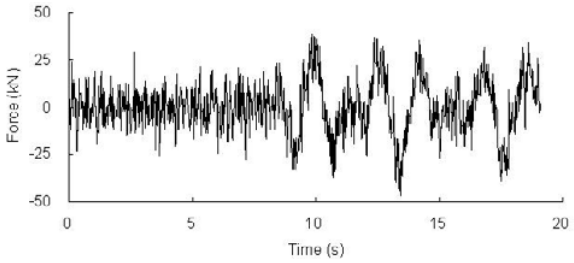

(b) seismic intensity V

Fig. 12. Lateral wheel-rail force histories with and without seismic loads.

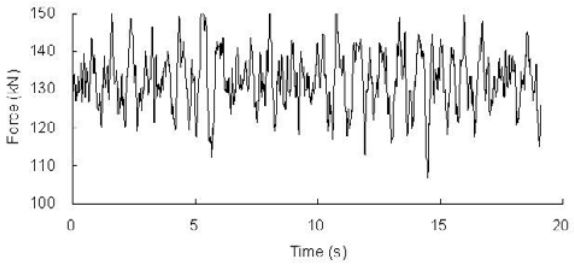

(a) without seismic load

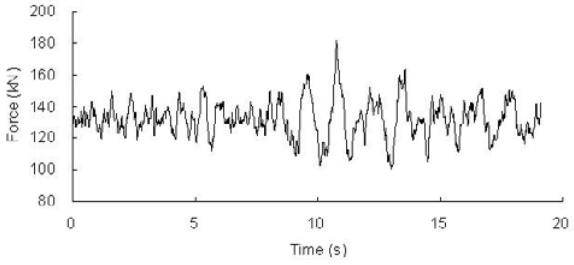

(b) seismic intensity V

Fig. 13. Vertical wheel-rail force histories with and without seismic loads.

isting in the lateral and vertical wheel-rail force histories during the peak of seismic excitation. The maximum lateral and vertical wheel-rail forces increased 1.59 times and 1.16 times due to the seismic load with intensity V.

As safety factors, the derailment factor and the offloading factor are chosen as controlling indexes in many countries, and are defined as

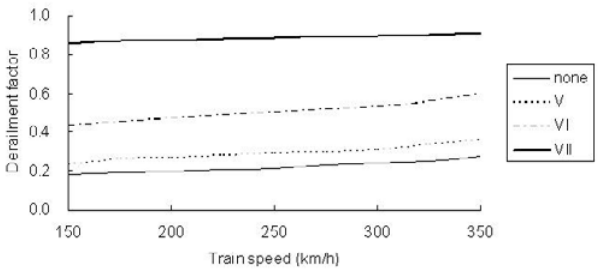

Fig. 14. Derailment factor vs. train speed.

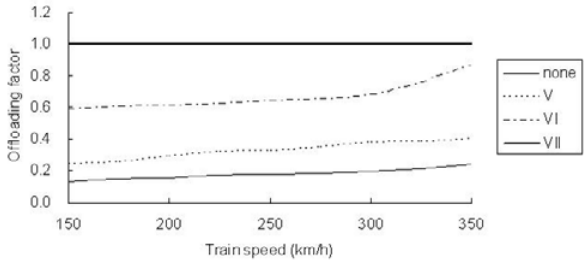

Fig. 15. Offloading factor vs. train speed.

$$\text{derailment factor} = \frac{|Q|}{P} \tag{12}$$

$$\text{offloading factor} = \begin{cases} 0 & P \geq P_S \\ \dfrac{P_S - P}{P_S} & P < P_S \end{cases} \tag{13}$$

where Q and P are the lateral and vertical wheel-rail interaction forces for an individual wheel (referring not to the total interaction force of a wheel-set but to the force of a single wheel at the left or right contact point), and P_S is the static weight of that individual wheel.

The relations of the derailment and offloading factors versus train speed with the different seismic intensities are shown in Figs. 14 and 15.

The figures indicate that that these vehicle safety factors increased markedly with the seismic intensity. The derailment factors with seismic intensity VII, and the offloading factors with seismic intensities VI and VII, exceeded the limitations listed in Reference [1] in most cases, which are 0.8 for the derailment factor and 0.6 for the offloading factor. Thus, trains must decrease their speed or even stop when an earthquake of seismic intensity VI or greater occurs.

The commonly accepted vertical and lateral acceleration limitations for high-speed trains are 0.13 g and 0.10 g respectively, according to the Track Irregularity Administration Standard in China [1]. These ensure the comfort of passengers, and can be ignored when earthquakes occur. For this reason, train acceleration was not considered in the case study.

4. Conclusions

This paper proposes a method to simulate dynamic responses of the vehicle-bridge interaction system under multi-

support seismic excitation, in which method the seismic acceleration history is incorporated by the large mass method to ensure bridge foundations have their specific dynamic status. The following conclusions for a case study could be drawn:

(1) The bridge vibration, the wheel-rail interaction force and the vehicle safety factors increased with the seismic intensity and the train speed.

(2) Earthquake excitation contributes more than track-irregularity excitation to the vehicle-bridge interaction system.

(3) Bridge responses induced by seismic excitation have lower-frequency components than those induced by track irregularities, and the seismic load affects bridge vibration in the lateral direction more than that in the vertical direction.

(4) The derailment factors and offloading factors increase markedly with the seismic intensity. The derailment factors with seismic intensity VII, and the offloading factors with seismic intensities VI and VII, exceeded the limitation listed. Therefore, trains must decrease their speed or even stop when an earthquake of seismic intensity VI or greater occurs.

Acknowledgement

This ongoing research is supported by the Natural Science Foundation of China (Grant Nos. 90715008, 50838006) and the Flanders (Belgium) - China bilateral project (No. BIL 07/07).

References

[1] H. Xia and N. Zhang, *Dynamic interaction of vehicle and structures* (2nd Edition), Beijing: Science Press (2005).

[2] J. D. Yau and Y. B. Yang, Vibration of a suspension bridge installed with a water pipeline and subjected to moving trains, *Engineering Structures*, 30 (3) (2008) 632-642.

[3] S. H. Ju and H. T. Lin, Resonance characteristics of high-speed trains passing simply supported bridges, *J Sound and Vibration*, 267 (2003) 1127-1141.

[4] H. Lob and D. K. Bao, An efficient analysis of structural response for multiple-support seismic excitations, *Engineering Structure*, 17 (1) (1995) 15-26.

[5] G. Monti, C. Nuti and P. Pinto, Nonlinear response of bridges under multi-supported excitations, *J Structural Engineering*, 122 (10) (1996) 1147-1159.

[6] J. W. Miao, S. D. Hu and L. C. Fan, State of art and development of study on seismic performance of long span bridges under multiple-support excitations, *J Tongji University*, 27 (2) (1999) 189-193.

[7] P. Leger , I. M. Ide and P. Pauhre, Multiple-support seismic analysis of large structures, *Computers & Structures*, 36 (6) (1990) 153-158.

[8] L. W. Edward, *Three-dimensional static and dynamic analysis of structures* (3rd Edition), CA: Computer and Structures, Inc. (2002).

[9] D. Kiureghian and A. Neuenhofer, Response spectrum method for multi-support seismic excitations, *Earthquake Engineering and Structural Dynamics*, 21 (1992) 713-740.

[10] D. Kiureghian and A. Neuenhofer, Discussion on seismic random-vibration analysis of multi-support structure systems, *J Mechanics Engineering*, ASCE, 121 (9) (1995) 1037.

[11] E. Heredia-Zavoni and E. H. Vanmarcke, Seismic random-vibration analysis of multi-support structure systems, *J Mechanics Engineering*, ASCE, 120 (5) (1994) 1107-1128.

[12] E. Heredia-Zavoni and E. H. Vanmarcke, Closure on the discussion on seismic random-vibration analysis of multi-support structure systems, *J Mechanics Engineering*, ASCE, 121 (9) (1995) 1037-1038.

[13] J. H. Lin and Y. H. Zhang, *Pseudo-excitation in Random Vibration*, Beijing: Science Press (2004).

[14] N. Zhang, H. Xia H and W. W. Guo, Vehicle-bridge Interaction Analysis under High-speed Trains, *J Sound and Vibration*, 309 (2008) 407-425.

[15] F. T. Wang, *Vehicle Dynamics*, Beijing: China Railway Press (1994).

[16] N. Zhang, H. Xia and G. De Roeck, Spectrum and sensitivity analysis of vehicle-bridge interaction system, *Proc. ISEV2007*, Taipei, (2007) 357-362.

[17] W. M. Zhai, *Vehicle-track coupling dynamics* (3rd Edition), Beijing: Science Press (2007).

Nan Zhang was awarded a Ph.D. degree in Bridge and Tunnel En-gineering in 2002. He is an associate professor in the School of Civil Engineering, Beijing Jiaotong University, China. His academic interests are vehicle-bridge interaction analysis, bridge design theory, structural dynamics and the finite element method.